ACS Catalysis

pubs.acs.org/acscatalysis Letter

The Dynamic Structure of $Au_{38}(SR)_{24}$ Nanoclusters Supported on CeO_2 upon Pretreatment and CO Oxidation

Stephan Pollitt, Vera Truttmann, Thomas Haunold, Clara Garcia, Wojciech Olszewski, Jordi Llorca, Noelia Barrabés,* and Günther Rupprechter

Cite This: *ACS Catal.* 2020, 10, 6144–6148

Read Online

ACCESS | Metrics & More | Article Recommendations | Supporting Information

ABSTRACT: Atomically precise thiolate protected Au nanoclusters $Au_{38}(SC_2H_4Ph)_{24}$ on CeO_2 were used for in-situ (operando) extended X-ray absorption fine structure/diffuse reflectance infrared fourier transform spectroscopy and ex situ scanning transmission electron microscopy−high-angle annular dark-field imaging/X-ray photoelectron spectroscopy studies monitoring cluster structure changes induced by activation (ligand removal) and CO oxidation. Oxidative pretreatment at 150 °C "collapsed" the clusters' ligand shell, oxidizing the hydrocarbon backbone, but the S remaining on Au acted as poison. Oxidation at 250 °C produced bare Au surfaces by removing S which migrated to the support (forming Au^+-S), leading to highest activity. During reaction, structural changes occurred via CO-induced Au and O-induced S migration to the support. The results reveal the dynamics of nanocluster catalysts and the underlying cluster chemistry.

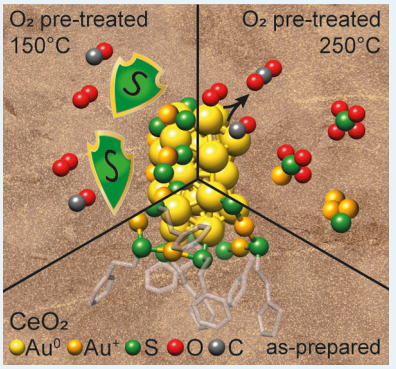

KEYWORDS: *Au nanoclusters, catalysis, in situ XAFS, DRIFTS, CeO_2*

A great challenge in nanocatalysis is to produce truly homogeneous, structurally well-defined, and highly active nanostructures that can serve for fundamental studies and new applications. Thiolate-protected metal nanoclusters ($M_n(SR)_m$) with well-defined structures offer a route toward creating atomically precise and catalytically active sites,[1−4] providing model systems for atomic level studies of catalytic properties.[3,5,6]

It is well-accepted that Au clusters (with <100 Au atoms) supported by metal oxides exhibit excellent catalytic activity for (low temperature) oxidation[4,7−14] and hydrogenation,[15−17] especially when compared with larger Au nanoparticles. Au clusters facilitate reactant activation due to higher adsorption energies. Nevertheless, the initially well-defined Au cluster structure may change during pretreatment and reaction, which is also affected by cluster size and the type of support material.[18−21] Previously, we have studied structural changes of Au clusters of different size, that is, $Au_x(SC_2H_4Ph)_y$ (x = 25, 38, and 144, y = 18, 24, and 60) supported on metal oxides (CeO_2, Al_2O_3, and SiO_2) upon oxidative pretreatment and liquid phase reaction. In situ X-ray absorption fine structure spectroscopy (XAFS) and high-energy resolution fluorescence detected−X-ray absorption spectroscopy (HERFD-XAS) revealed higher cluster stability on CeO_2 and SiO_2[21−23] than on Al_2O_3. Here, we refine the structural picture on cluster chemistry by in situ/operando extended X-ray absorption fine structure (EXAFS) and diffuse reflectance infrared fourier transform spectroscopy (DRIFTS), to directly monitor the dynamic structure of $Au_{38}(SC_2H_4Ph)_{24}$ clusters on CeO_2, both during ligand removal and CO oxidation.

CO oxidation has been repeatedly used to assess the catalytic properties/active sites of (mainly CeO_2) supported thiolated gold nanoclusters, particularly addressing ligand effects.[14,18,24−28] Two different mechanisms were proposed: (i) Mars−van Krevelen, with CO adsorbed on Au and active oxygen provided by CeO_2 at the metal/oxide interface,[29] which was supported by Good et al. showing that the reaction of oxygen from the ceria lattice with CO adsorbed on gold was the rate limiting step;[30] (ii) Langmuir−Hinshelwood, with CO and O coadsorbed on neighboring Au sites.[31] Lopez Acevedo et al. explained the catalytic activity of thiolate protected gold nanoclusters with their HOMO−LUMO energy gap, which matches the binding energy of oxygen on Au.[31] Hence, for $Au_{38}(SR)_{24}$ clusters only the removal of ligands turns them into electropositive species that are able to adsorb O_2. A combination of activated adsorbed and lattice oxygen provides ideal conditions for reaction with adsorbed CO.

Jin and co-workers proposed that not the bulkiness of the hydrocarbon tails but the ligands at the interface between

Received: April 9, 2020
Revised: May 8, 2020
Published: May 8, 2020

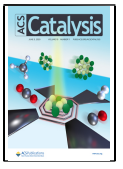

thiolated Au clusters and CeO_2 inhibited CO adsorption on Au and reaction with lattice O, hence adversely affecting CO oxidation.[25] Accordingly, pretreatments removing the ligand shell should have a positive effect on activity.

Nie et al.[27,28] reported for $Au_n(SR)_m/CeO_2$ (n = 25, 38, m = 18, 24) that partial thiolate (ligand) removal led to higher activity than complete ligand removal. According to Wu et al.,[26] partial removal of thiol ligands by oxidation around 150 °C enabled CO adsorption on the exposed Au surface,[26,27] whereas full removal did not have any further effect.[26] Overall, the effect of thiolate ligands and their removal on the catalytic activity of Au nanoclusters is still controversially discussed.[1,4,14,18,21,25,30,32]

Recently, we have reported a new effect, that is, migration of thiolate ligands from the Au clusters to the supporting oxide.[23] Although the assumption had been that thiolate ligands "disappeared" into the gas phase upon oxidative activation, S K-edge XAFS measurements detected that oxidized sulfur species remained on the support.[23] The redistribution and oxidation of S modified the support, which may also alter its catalytic function (e.g., by poisoning interface sites or vacancies).

Herein, we performed more detailed in situ/operando EXAFS/DRIFTS and ex situ scanning transmission electron microscopy−high-angle annular dark-field imaging/X-ray photoelectron spectroscopy (STEM-HAADF/XPS) studies of structural changes of $Au_{38}(SR)_{24}/CeO_2$ upon pretreatment and CO oxidation. In situ XAFS Au L_3-edge spectra of $Au_{38}(SR)_{24}/CeO_2$ upon different oxidative pretreatment indicated that not only ligands were removed but also that staples collapsed, depositing S atoms on the Au surface (poisoning). At higher temperature, S species migrated from the Au clusters to the support, creating bare active Au surfaces. During CO oxidation, further structural changes occurred via CO-induced Au and O-induced S migration to the support. The complex temperature dependence of these structural changes and the formation of Au−S units may explain the conflicting reports in literature on the effect of pretreatment on catalytic properties.

The atomic structure of $Au_{38}(SC_2H_4Ph)_{24}$ was previously solved by X-ray crystallography,[33] with EXAFS confirmation thereafter.[34−36] The $Au_{38}(SR)_{24}$ nanoclusters consist of a symmetric biicosahedral structure Au_{23} core, which is protected by three monomeric (SR-Au-SR) and six dimeric staples (SR-Au-SR-Au-SR; Scheme 1).

As mentioned, oxidative catalyst activation is required and the structural evolution of CeO_2 supported $Au_{38}(SR)_{24}$ nanoclusters were studied by Au L_3-edge XAS (Figure 1).

Scheme 1. $Au_{38}(SR)_{24}$ Nanocluster (Initial) Structure with Distances Fitted by EXAFS

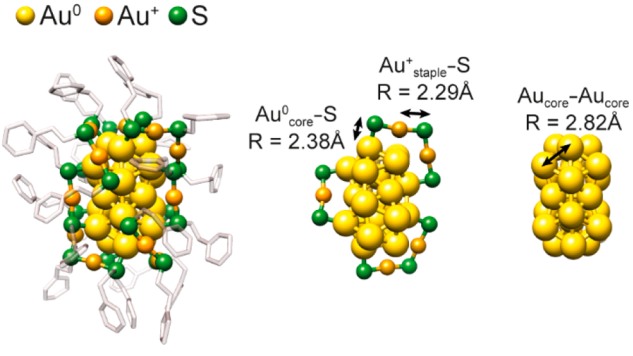

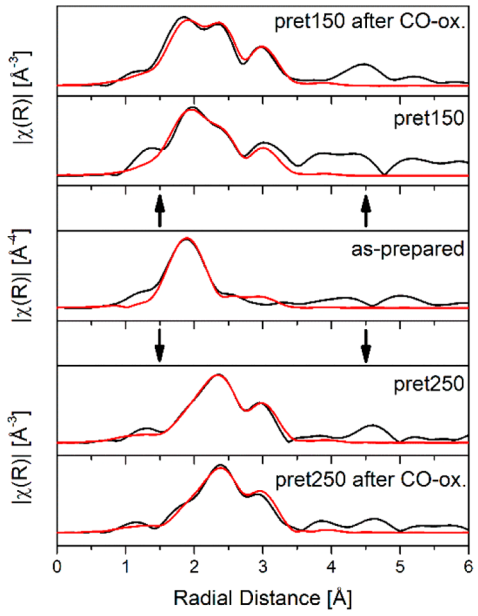

Figure 1. EXAFS fit (red) in R space of the as-prepared sample, after pretreatment (150 or 250 °C, in 5% O_2 in He) and after CO oxidation reaction.

The Artemis package[37] using the FEFF8 code[38] was applied for EXAFS data treatment, building a cluster model based on the known crystal structure. The fitted values of the three key distances are illustrated in Scheme 1. The Au−Au distance characterizes neighboring Au atoms (e.g., those in the core). There are two different Au−S bond distances, one corresponding to Au^0_{core}-S and the other to Au^+_{staple}-S.

The cluster's structural changes upon pretreatment were evaluated via two main EXAFS parameters: R (distance) and N (coordination number of neighboring equivalent atoms). Table S1 and Figure S3 collect the fitting results, while the deduced structural changes are illustrated in Scheme 2.

As expected, the number of nearest equivalent Au neighbors (N_{Au-Au}) increased upon pretreatment (2.59 to 5.08 or 8.09), because of the increasing removal of the ligands, but EXAFS analysis still suggested that the core structure was preserved. However, the N values of Au^0_{core}-S and Au^+_{staple}-S, which are expected to continuously decrease upon pretreatment, showed

Scheme 2. Evolution of the $Au_{38}(SR)_{24}/CeO_2$ Cluster Structure Derived from EXAFS Fit, after Pretreatment at 150 or 250°C and Subsequent CO Oxidation

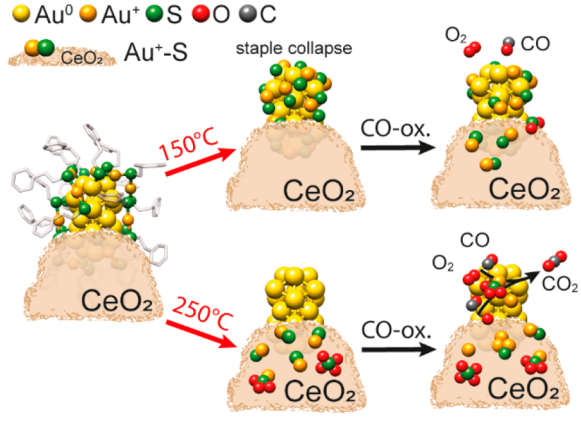

https://dx.doi.org/10.1021/acscatal.0c01621
ACS Catal. 2020, 10, 6144−6148

a deviating behavior. Apparently, the structural changes are more complex than just a simple successive removal of (entire) ligands.

When $Au_{38}(SR)_{24}/CeO_2$ was pretreated at 150 °C, the Au−Au and Au−S distances (R) did not change. In line with ligand removal, N of Au−Au increased and N Au^{+}_{staple}-S strongly decreased, but N Au^{0}_{core}-S unexpectedly increased. The removal of the thiolate carbon backbone seems to collapse the remaining staples, creating new bonds between Au−Au but also between the outer Au atoms of the cluster core and S (Au^{0}_{core}-S). Pretreatment at 250 °C almost completely removed S from the cluster core, as N Au^{0}_{core}-S became almost zero. However, N Au^{+}_{staple}-S was still 0.45, indicating creation of Au^{+}-S configurations, which can only be on the support (staples collapsed at 150 °C not reestablished at 250 °C).

Figure 2 shows catalytic CO oxidation, comparing pretreated $Au_{38}(SR)_{24}/CeO_2$ with CeO_2. Catalytic activity was monitored

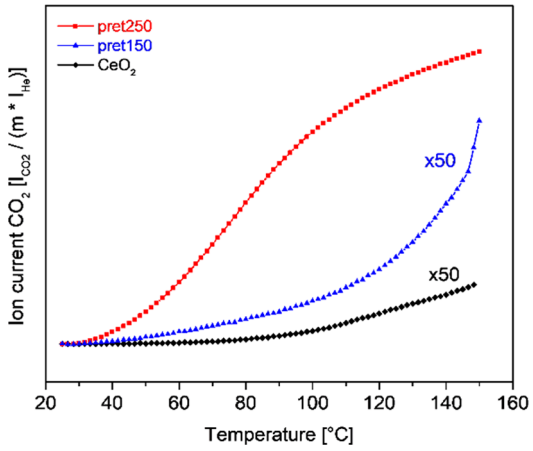

Figure 2. CO oxidation on 2 wt % $Au_{38}(SR)_{24}$ supported on CeO_2 (flow: 3.3% CO, 7% O_2, 89.7% He, total flow: 60 mL/min, ramp: 5 °C/min): CO_2 MS traces normalized to the catalyst mass and the He signal, after different pretreatments, and for the pure support.

by a mass spectrometer (MS) connected to the reaction cell outlet. $Au_{38}(SR)_{24}/CeO_2$ pretreated at 150 °C showed only minute activity even at 150 °C. This confirms the structural model, as Au atoms blocked by S were inaccessible for CO and O_2 adsorption.

In contrast, $Au_{38}(SR)_{24}/CeO_2$ pretreated at 250 °C was active even below 40 °C, being more than 50-times more active than the catalyst sample pretreated at 150 °C (pret150). Again, this confirms the structural model of bare Au surfaces, as Au^{+}-S species are inactive. The as-prepared $Au_{38}(SR)_{24}/CeO_2$ catalyst with intact ligands was nearly inactive and also sintered, losing the cluster monodispersity; therefore, it will not be further considered here.

In order to investigate reaction-induced structural changes, the samples were again characterized by EXAFS after CO oxidation (Table S1 and Figure S3). During reaction on the catalyst sample pretreated at 250 °C (pret250), the Au core structure present after pretreatment was preserved, indicated by the only slightly reduced Au−Au coordination numbers, the bond distances and EXAFS fitting (minimal change of σ_0^2Au−Au).

However, N Au^{+}_{staple}-S decreased and N Au^{0}_{core}-S increased during the reaction. As S migration back to the cluster is unlikely, this suggests that (isolated) Au^{+}_{staple}-S converted to (agglomerated) Au^{0}_{core}-S on the support and/or that Au^{+}_{staple}-S dissociated. Additionally, more Au atoms may move to the support and merge with S species. Migration of Au atoms under reaction conditions can be explained by CO-induced atom mobility, as observed before,[39−41] which explains the decrease of N Au−Au. Accordingly, S species are mobile not only during pretreatment, as shown by our previous XANES study,[23] but also during the catalytic reaction. The two Au−S species will not contribute to catalytic activity, as S is a strong poison. During CO oxidation on the less active pret150 sample with initially S-poisoned Au surfaces, S moved to the support (decreasing N Au^{0}_{core}-S and increasing N Au−Au) and merged with CO-mobilized Au atoms (increasing N Au^{+}_{staple}-S). However, during reaction at 150 °C activity did not increase significantly. S may be removed from the clusters, but it will still poison the surrounding ceria.

To address morphological changes, STEM-HAADF images were acquired for the "as-prepared" catalyst and the catalysts after CO oxidation (Figure S6). In all cases, Au nanoclusters of 2−4 nm size were identified. Smaller entities, like Au−S particles formed by migration of Au and S species during reaction (as indicated by N Au^{+}_{staple}-S) may be present as well but were beyond detection.

Possible reaction-induced changes in the Au oxidation state were studied by X-ray photoelectron spectroscopy (XPS) (Figure S7). For the as-prepared sample, the Au $4f_{7/2}$ signal at 84.2 eV is characteristic of ceria supported Au clusters that are modified by metal−ligand interaction. For ligand-free Au^0 nanoclusters on ceria,[42,43] a binding energy of 83.8 eV was reported by Huang et al.[23,44,45] After pretreatment and reaction, the Au 4f signals were shifted to lower binding energies. For the pret150 catalyst, the small shift agrees with the collapse of the staples, while for the pret250 sample, the −0.3 eV shift corroborates the formation of bare Au^0 clusters.

To monitor adsorbed species, in situ diffuse reflectance infrared Fourier transform spectroscopy (DRIFTS) was performed during CO oxidation. Figure 3 displays temper-

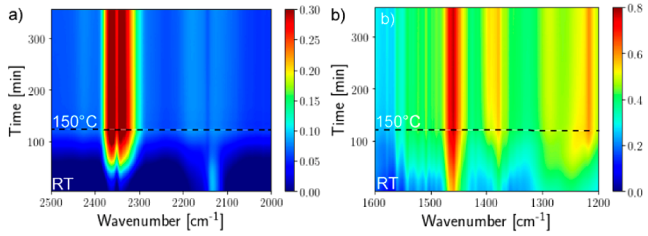

Figure 3. Operando DRIFTS during CO oxidation on Au_{38}/CeO_2 pretreated at 250 °C, from room temperature to 150 °C (background corrected with pure CeO_2 pretreated under the same conditions). (a) 2500−2000 cm^{-1}, (b) 1600−1200 cm^{-1}.

ature-dependent operando DRIFTS measurements of the highly active $Au_{38}(SR)_{24}/CeO_2$ catalyst pretreated at 250 °C. Spectra were taken from room temperature to 150 °C (ramp 1 °C/min, then isothermal for 4 h).

CO adsorbed on Au^0 (2130 cm^{-1}) was observed below 118 °C, corroborating clean Au surfaces (Figure S8). CO_2 formation was already observed at room temperature by MS (Figure S12) and gas-phase bands between 2300 and 2400 cm^{-1} (Figures 3a and S9). In the lower wavenumber region (Figure 3b), the typical monodentate carbonates, frequently

https://dx.doi.org/10.1021/acscatal.0c01621
ACS Catal. 2020, 10, 6144−6148

observed during CO oxidation and bonded to ceria, were observed via an increasing signal at 1468 cm^{-1}. For sulfation of CeO_2, Waqif et al. reported distinct IR bands of surface SO_3 (or $S_2O_7^{-2}$) and SO_4 (1x S = O, 3x S−O−Ce),[46] which were also present here (Figures S10 and S11). Bulk SO_4 was absent (missing bands at 1196, 1128 cm^{-1} in Figure S11).[46,47] Surface SO_3 and SO_4 increased over time, becoming more pronounced close to maximum temperature in Figure 3b. Thus, sulfur from Au−S species, which have migrated to the support during pretreatment, reacted to surface SO_3 and SO_4.

The detailed evolution of the structure of $Au_{38}(SR)_{24}$ nanoclusters supported on CeO_2 was monitored upon pretreatment and CO oxidation. Whereas unpretreated samples tend to sinter, oxidative pretreatment at 150 °C collapsed the staples structure. Unlike the hydrocarbon backbone, sulfur was not removed to the gas phase but remained on the Au core, thus inhibiting adsorption of CO and oxygen. Pretreatment at 250 °C fully removed S and created clean Au^0 clusters with intact core structure. The removal of ligands was beneficial for CO oxidation, which is why the pret250 sample had the highest activity, being already active at room temperature. During reaction, mobile Au and S species formed additional (inactive) Au−S entities. Operando DRIFTS detected CO adsorption on Au^0 below 118 °C, in addition to carbonates on the ceria support. A slow continuous transformation to SO_3 and SO_4 was observed (during ∼6 h), becoming more pronounced close to the maximum temperature. The current results are particularly relevant for further studies of cluster chemistry and functionality. It is important to understand the role and fate of staples/ligands and their interaction with the support, as this strongly affects catalytic performance.

■ ASSOCIATED CONTENT

Supporting Information

The Supporting Information is available free of charge at https://pubs.acs.org/doi/10.1021/acscatal.0c01621.

Synthesis procedures and catalyst preparation; EXAFS; Kinetics; STEM-HAADF; XPS; DRIFTS (PDF)

■ AUTHOR INFORMATION

Corresponding Author

Noelia Barrabés − *Institute of Materials Chemistry, TU Wien, 1060 Vienna, Austria;* orcid.org/0000-0002-6018-3115; Phone: +43 (1) 58801 165109; Email: noelia.rabanal@tuwien.ac.at

Authors

Stephan Pollitt − *Institute of Materials Chemistry, TU Wien, 1060 Vienna, Austria*

Vera Truttmann − *Institute of Materials Chemistry, TU Wien, 1060 Vienna, Austria*

Thomas Haunold − *Institute of Materials Chemistry, TU Wien, 1060 Vienna, Austria*

Clara Garcia − *Institute of Materials Chemistry, TU Wien, 1060 Vienna, Austria*

Wojciech Olszewski − *ALBA Synchrotron Light Facility, 08290 Cerdanyola del Vallés, Barcelona, Spain; Faculty of Physics, University of Bialystok, Bialystok, Poland*

Jordi Llorca − *Institute of Energy Technologies, Department of Chemical Engineering and Barcelona Research Center in Multiscale Science and Engineering, Universitat Politècnica de Catalunya EEBE, 08019 Barcelona, Spain;* orcid.org/0000-0002-7447-9582

Günther Rupprechter − *Institute of Materials Chemistry, TU Wien, 1060 Vienna, Austria;* orcid.org/0000-0002-8040-1677

Complete contact information is available at: https://pubs.acs.org/10.1021/acscatal.0c01621

Author Contributions

Sample preparations were performed by S.P. and C.G. EXAFS measurements were performed by N.B., V.T. and S.P. EXAFS fitting was carried out by W.O. Operando DRIFTS measurements and data analysis were done by S.P. XPS measurements and analysis was carried out by T.H. and V.T. STEM-HAADF measurements with analysis were performed by J.L. Final interpretation and manuscript preparation was led by S.P., N.B. and G.R., with contributions of all authors. Funding was acquired by G.R.

Notes

The authors declare no competing financial interest.

■ ACKNOWLEDGMENTS

GR acknowledges financial support by the Austrian Science Fund (FWF) via grants ComCat (I1041−N28) and DK+ Solids4Fun (W1243). We thank Prof. T. Bürgi's research group for help during the synchrotron measurements. ALBA synchrotron is acknowledged for beamtime at the CLAESS beamline (Proposal ID: 2016091918). J.L. is a Serra Húnter Fellow and is grateful to ICREA Academia program and GC 2017 SGR 128.

■ REFERENCES

(1) Zhao, J.; Jin, R. Heterogeneous catalysis by gold and gold-based bimetal nanoclusters. *Nano Today* **2018**, *18*, 86−102.

(2) Jin, R. C.; Zeng, C. J.; Zhou, M.; Chen, Y. X. Atomically Precise Colloidal Metal Nanoclusters and Nanoparticles: Fundamentals and Opportunities. *Chem. Rev.* **2016**, *116*, 10346−10413.

(3) Liu, L.; Corma, A. Metal Catalysts for Heterogeneous Catalysis: From Single Atoms to Nanoclusters and Nanoparticles. *Chem. Rev.* **2018**, *118*, 4981−5079.

(4) Yamazoe, S.; Koyasu, K.; Tsukuda, T. Nonscalable Oxidation Catalysis of Gold Clusters. *Acc. Chem. Res.* **2014**, *47*, 816−824.

(5) Cui, X.; Li, W.; Ryabchuk, P.; Junge, K.; Beller, M. Bridging homogeneous and heterogeneous catalysis by heterogeneous single-metal-site catalysts. *Nature Catalysis* **2018**, *1*, 385−397.

(6) Higaki, T.; Li, Y.; Zhao, S.; Li, Q.; Li, S.; Du, X.-S.; Yang, S.; Chai, J.; Jin, R. Atomically Tailored Gold Nanoclusters for Catalytic Application. *Angew. Chem., Int. Ed.* **2019**, *58*, 8291−8302.

(7) Liu, Y. M.; Tsunoyama, H.; Akita, T.; Xie, S. H.; Tsukuda, T. Aerobic Oxidation of Cyclohexane Catalyzed by Size-Controlled Au Clusters on Hydroxyapatite: Size Effect in the Sub-2 nm Regime. *ACS Catal.* **2011**, *1*, 2−6.

(8) Yamazoe, S.; Yoskamtorn, T.; Takano, S.; Yadnum, S.; Limtrakul, J.; Tsukuda, T. Controlled Synthesis of Carbon-Supported Gold Clusters for Rational Catalyst Design. *Chem. Rec* **2016**, *16*, 2338−2348.

(9) Haruta, M. Catalysis - Gold rush. *Nature* **2005**, *437*, 1098−1099.

(10) Luo, J.; Jones, V. W.; Maye, M. M.; Han, L.; Kariuki, N. N.; Zhong, C.-J. Thermal Activation of Molecularly-Wired Gold Nanoparticles on a Substrate as Catalyst. *J. Am. Chem. Soc.* **2002**, *124*, 13988−13989.

(11) Tsunoyama, H.; Ichikuni, N.; Sakurai, H.; Tsukuda, T. Effect of Electronic Structures of Au Clusters Stabilized by Poly(N-vinyl-2-pyrrolidone) on Aerobic Oxidation Catalysis. *J. Am. Chem. Soc.* **2009**, *131*, 7086−7093.

(12) Gajan, D.; Guillois, K.; Delichère, P.; Basset, J.-M.; Candy, J.-P.; Caps, V.; Coperet, C.; Lesage, A.; Emsley, L. Gold Nanoparticles Supported on Passivated Silica: Access to an Efficient Aerobic Epoxidation Catalyst and the Intrinsic Oxidation Activity of Gold. *J. Am. Chem. Soc.* **2009**, *131*, 14667−14669.
(13) Wang, Q.; Yeung, K. L.; Bañares, M. A. Operando Raman-online FTIR investigation of ceria, vanadia/ceria and gold/ceria catalysts for toluene elimination. *J. Catal.* **2018**, *364*, 80−88.
(14) Yoskamtorn, T.; Yamazoe, S.; Takahata, R.; Nishigaki, J.-i.; Thivasasith, A.; Limtrakul, J.; Tsukuda, T. Thiolate-Mediated Selectivity Control in Aerobic Alcohol Oxidation by Porous Carbon-Supported Au25Clusters. *ACS Catal.* **2014**, *4*, 3696−3700.
(15) Zhu, Y.; Qian, H.; Zhu, M.; Jin, R. Thiolate-Protected Aun Nanoclusters as Catalysts for Selective Oxidation and Hydrogenation Processes. *Adv. Mater.* **2010**, *22*, 1915−1920.
(16) Li, G.; Jiang, D.-e.; Kumar, S.; Chen, Y.; Jin, R. Size Dependence of Atomically Precise Gold Nanoclusters in Chemoselective Hydrogenation and Active Site Structure. *ACS Catal.* **2014**, *4*, 2463−2469.
(17) Zhu, Y.; Qian, H.; Drake, B. A.; Jin, R. Atomically Precise Au25(SR)18 Nanoparticles as Catalysts for the Selective Hydrogenation of α,β-Unsaturated Ketones and Aldehydes. *Angew. Chem.* **2010**, *122*, 1317−1320.
(18) Zhang, B.; Kaziz, S.; Li, H.; Hevia, M. G.; Wodka, D.; Mazet, C.; Burgi, T.; Barrabes, N. Modulation of Active Sites in Supported Au-38(SC2H4Ph)(24) Cluster Catalysts: Effect of Atmosphere and Support Material. *J. Phys. Chem. C* **2015**, *119*, 11193−11199.
(19) Sudheeshkumar, V.; Sulaiman, K. O.; Scott, R. W. J. Activation of atom-precise clusters for catalysis. *Nanoscale Advances* **2020**, *2*, 55−69.
(20) Sankar, M.; He, Q.; Engel, R. V.; Sainna, M. A.; Logsdail, A. J.; Roldan, A.; Willock, D. J.; Agarwal, N.; Kiely, C. J.; Hutchings, G. J. Role of the Support in Gold-Containing Nanoparticles as Heterogeneous Catalysts. *Chem. Rev.* **2020**, *120*, 3890−3938.
(21) García, C.; Pollitt, S.; van der Linden, M.; Truttmann, V.; Rameshan, C.; Rameshan, R.; Pittenauer, E.; Allmaier, G.; Kregsamer, P.; Stöger-Pollach, M.; Barrabés, N.; Rupprechter, G. Support effect on the reactivity and stability of Au25(SR)18 and Au144(SR)60 nanoclusters in liquid phase cyclohexane oxidation. *Catal. Today* **2019**, *336*, 174−185.
(22) Zhang, B.; García, C.; Sels, A.; Salassa, G.; Rameshan, C.; Llorca, J.; Hradil, K.; Rupprechter, G.; Barrabés, N.; Bürgi, T. Ligand and support effects on the reactivity and stability of Au38(SR)24 catalysts in oxidation reactions. *Catal. Commun.* **2019**, *130*, 105768.
(23) Zhang, B.; Sels, A.; Salassa, G.; Pollitt, S.; Truttmann, V.; Rameshan, C.; Llorca, J.; Olszewski, W.; Rupprechter, G.; Bürgi, T.; Barrabés, N. Ligand Migration from Cluster to Support: A Crucial Factor for Catalysis by Thiolate-protected Gold Clusters. *ChemCatChem* **2018**, *10*, 5372−5376.
(24) Li, W.; Ge, Q.; Ma, X.; Chen, Y.; Zhu, M.; Xu, H.; Jin, R. Mild activation of CeO2-supported gold nanoclusters and insight into the catalytic behavior in CO oxidation. *Nanoscale* **2016**, *8*, 2378−2385.
(25) Li, Y.; Chen, Y.; House, S. D.; Zhao, S.; Wahab, Z.; Yang, J. C.; Jin, R. Interface Engineering of Gold Nanoclusters for CO Oxidation Catalysis. *ACS Appl. Mater. Interfaces* **2018**, *10*, 29425−29434.
(26) Wu, Z.; Jiang, D.-e.; Mann, A. K. P.; Mullins, D. R.; Qiao, Z.-A.; Allard, L. F.; Zeng, C.; Jin, R.; Overbury, S. H. Thiolate Ligands as a Double-Edged Sword for CO Oxidation on CeO2 Supported Au25(SCH2CH2Ph)18 Nanoclusters. *J. Am. Chem. Soc.* **2014**, *136*, 6111−6122.
(27) Nie, X. T.; Zeng, C. J.; Ma, X. G.; Qian, H. F.; Ge, Q. J.; Xu, H. Y.; Jin, R. C. CeO2-supported Au-38(SR)(24) nanocluster catalysts for CO oxidation: a comparison of ligand-on and -off catalysts. *Nanoscale* **2013**, *5*, 5912−5918.
(28) Nie, X. T.; Qian, H. F.; Ge, Q. J.; Xu, H. Y.; Jin, R. C. CO Oxidation Catalyzed by Oxide-Supported Au-25(SR)(18) Nanoclusters and Identification of Perimeter Sites as Active Centers. *ACS Nano* **2012**, *6*, 6014−6022.
(29) Kim, H. Y.; Lee, H. M.; Henkelman, G. CO Oxidation Mechanism on CeO2-Supported Au Nanoparticles. *J. Am. Chem. Soc.* **2012**, *134*, 1560−1570.
(30) Good, J.; Duchesne, P. N.; Zhang, P.; Koshut, W.; Zhou, M.; Jin, R. On the functional role of the cerium oxide support in the Au38(SR)24/CeO2 catalyst for CO oxidation. *Catal. Today* **2017**, *280*, 239−245.
(31) Lopez-Acevedo, O.; Kacprzak, K. A.; Akola, J.; Hakkinen, H. Quantum size effects in ambient CO oxidation catalysed by ligand-protected gold clusters. *Nat. Chem.* **2010**, *2*, 329−334.
(32) Wan, X.-K.; Wang, J.-Q.; Nan, Z.-A.; Wang, Q.-M. Ligand effects in catalysis by atomically precise gold nanoclusters. *Science Advances* **2017**, *3*, No. e1701823.
(33) Qian, H.; Eckenhoff, W. T.; Zhu, Y.; Pintauer, T.; Jin, R. Total Structure Determination of Thiolate-Protected Au38 Nanoparticles. *J. Am. Chem. Soc.* **2010**, *132*, 8280−8281.
(34) Yamazoe, S.; Tsukuda, T. X-ray Absorption Spectroscopy on Atomically Precise Metal Clusters. *Bull. Chem. Soc. Jpn.* **2019**, *92*, 193−204.
(35) Chevrier, D. M.; Yang, R.; Chatt, A.; Zhang, P. Bonding properties of thiolate-protected gold nanoclusters and structural analogs from X-ray absorption spectroscopy. *Nanotechnol. Rev.* **2015**, *4*, 193−206.
(36) Zhang, P. X-ray Spectroscopy of Gold−Thiolate Nanoclusters. *J. Phys. Chem. C* **2014**, *118*, 25291−25299.
(37) Ravel, B.; Newville, M. ATHENA, ARTEMIS, HEPHAESTUS: data analysis for X-ray absorption spectroscopy using IFEFFIT. *J. Synchrotron Radiat.* **2005**, *12*, 537−541.
(38) Rehr, J. J.; Albers, R. C. Theoretical approaches to x-ray absorption fine structure. *Rev. Mod. Phys.* **2000**, *72*, 621−654.
(39) Haghofer, A.; Sonström, P.; Fenske, D.; Föttinger, K.; Schwarz, S.; Bernardi, J.; Al-Shamery, K.; Bäumer, M.; Rupprechter, G. Colloidally Prepared Pt Nanowires versus Impregnated Pt Nanoparticles: Comparison of Adsorption and Reaction Properties. *Langmuir* **2010**, *26*, 16330−16338.
(40) Roiaz, M.; Falivene, L.; Rameshan, C.; Cavallo, L.; Kozlov, S. M.; Rupprechter, G. Roughening of Copper (100) at Elevated CO Pressure: Cu Adatom and Cluster Formation Enable CO Dissociation. *J. Phys. Chem. C* **2019**, *123*, 8112−8121.
(41) Gong, X.-Q.; Selloni, A.; Dulub, O.; Jacobson, P.; Diebold, U. Small Au and Pt Clusters at the Anatase TiO2(101) Surface: Behavior at Terraces, Steps, and Surface Oxygen Vacancies. *J. Am. Chem. Soc.* **2008**, *130*, 370−381.
(42) Huang, X. S.; Sun, H.; Wang, L. C.; Liu, Y. M.; Fan, K. N.; Cao, Y. Morphology effects of nanoscale ceria on the activity of Au/CeO2 catalysts for low-temperature CO oxidation. *Appl. Catal., B* **2009**, *90*, 224−232.
(43) Casaletto, M. P.; Longo, A.; Martorana, A.; Prestianni, A.; Venezia, A. M. XPS study of supported gold catalysts: the role of Au0 and Au+δ species as active sites. *Surf. Interface Anal.* **2006**, *38*, 215−218.
(44) Bourg, M.-C.; Badia, A.; Lennox, R. B. Gold-Sulfur Bonding in 2D and 3D Self-Assembled Monolayers: XPS Characterization. *J. Phys. Chem. B* **2000**, *104*, 6562−6567.
(45) Zhang, B.; Kaziz, S.; Li, H. H.; Wodka, D.; Malola, S.; Safonova, O.; Nachtegaal, M.; Mazet, C.; Dolamic, I.; Llorca, J.; Kalenius, E.; Daku, L. M. L.; Hakkinen, H.; Burgi, T.; Barrabes, N. Pd2Au36-(SR)(24) cluster: structure studies. *Nanoscale* **2015**, *7*, 17012−17019.
(46) Waqif, M.; Bazin, P.; Saur, O.; Lavalley, J. C.; Blanchard, G.; Touret, O. Study of ceria sulfation. *Appl. Catal., B* **1997**, *11*, 193−205.
(47) Chang, H.; Ma, L.; Yang, S.; Li, J.; Chen, L.; Wang, W.; Hao, J. Comparison of preparation methods for ceria catalyst and the effect of surface and bulk sulfates on its activity toward NH3-SCR. *J. Hazard. Mater.* **2013**, *262*, 782−788.

https://dx.doi.org/10.1021/acscatal.0c01621
ACS Catal. 2020, 10, 6144−6148